

Check for updates

www.aiii-jouinai.de

Highly Deformable Rigid Glassy Conjugated Polymeric Thin Films

Yunfei Wang, Song Zhang, Guillaume Freychet, Zhaofan Li, Kai-Lin Chen, Chih-Ting Liu, Zhiqiang Cao, Yu-Cheng Chiu, Wenjie Xia, and Xiaodan Gu*

Wearable devices benefit from the use of stretchable conjugated polymers (CPs). Traditionally, the design of stretchable CPs is based on the assumption that a low elastic modulus (E) is crucial for achieving high stretchability. However, this research, which analyzes the mechanical properties of 65 CP thin films, challenges this notion. It is discovered that softness alone does not determine stretchability; rather, it is the degree of entanglement that is critical. This means that rigid CPs can also exhibit high stretchability, contradicting conventional wisdom. To inverstigate further, the mechanical behavior, electrical properties, and deformation mechanism of two model CPs: a glassy poly(3-butylthiophene-2,5-diyl) (P3BT) with an E of 2.2 GPa and a viscoelastic poly(3-octylthiophene-2,5-diyl) (P3OT) with an E of 86 MPa, are studied. Ex situ transmission X-ray scattering and polarized UV-vis spectroscopy revealed that only the initial strain (i.e., <20%) exhibits different chain alignment mechanisms between two polymers, while both rigid and soft P3ATs showed similarly behavior at larger strains. By challenging the conventional design metric of low E for high stretchability and highlighting the importance of entanglement, it is hoped to broaden the range of CPs available for use in wearable devices.

1. Introduction

Over the past decades, there has been remarkable progress in the development of stretchable semiconductors, which find applications in wearable and implantable devices such as electronic skins, personalized healthcare monitors, [1–5] wearable

smart displays,[6-8] and energy storage devices.[9] These wearable devices hold immense potential in the field of health sensors, as they can be directly attached to the human skin, offering convenience and accuracy. For seamless integration with the skin, the materials utilized in these devices must be deformable to accommodate the strains resulting from body motion. Conjugated polymers (CPs) have emerged as preferred materials for wearable devices due to their tunable chemical structures and compliant mechanical properties compared to their inorganic counterparts.[10-18] However, achieving high charge carrier mobility and high stretchability concurrently presents a challenge, as high charge carrier mobility often necessitates high crystallinity and chain rigidity, which tend to make the materials brittle.

In the pursuit of designing novel stretchable CPs, researchers have primarily focused on reducing the materials' elastic modulus, as it is widely believed that softer

materials offer higher stretchability.^[19] For example, intrinsically stretchable CPs were synthesized by incorporating conjugation-break spacers.^[20–27] or soft moieties.^[28–33] into the backbone and attaching longer or more flexible side chains.^[34–38] Another effective method involves blending CPs with soft and deformable elastomers, such as polydimethylsiloxane (PDMS), rubber, or

Y. Wang, S. Zhang, C.-T. Liu, Z. Cao, X. Gu School of Polymer Science and Engineering Center for Optoelectronic Materials and Devices The University of Southern Mississippi Hattiesburg, MS 39406, USA E-mail: xiaodan.gu@usm.edu G. Freychet National Synchrotron Light Source II Brookhaven National Lab Upton, NY 11973, USA G. Freychet University Grenoble Alpes

LETI Grenoble F-38000, France

The ORCID identification number(s) for the author(s) of this article can be found under https://doi.org/10.1002/adfm.202306576

DOI: 10.1002/adfm.202306576

Z. Li, W. Xia
Department of Civil
Construction and Environmental Engineering
North Dakota State University
Fargo, ND 58108, USA
K.-L. Chen, Y.-C. Chiu
Department of Chemical Engineering
National Taiwan University of Science and Technology
Taipei 106, Taiwan
W. Xia
Department of Aerospace Engineering
lowa State University
Ames, IA 50011, USA

www.afm-journal.de

1616282. Downloaded from https://onlineblargv.wiely.com/doi/10.1002/adfm.20236676 by Univ of California Lawrence Berkeley National Lab, Wikey Online Library on [28/11/2033]. See the Terms and Conditions (https://onlineblarg.wikey.com/terms-and-conditions) on Wikey Online Library for rules of use; OA articles are governed by the applicable Ceravive Commons

polystyrene-block-polyisoprene-block-polystyrene (SEBS), resulting in the fabrication of soft CP/elastomer composites.[39-46] These strategies have demonstrated success in achieving stretchability in CPs and have provided solutions for the development of innovative materials for various applications.

In recent work, Zheng et al. made a remarkable discovery demonstrating that indacenodithiophene-cobenzothiadiazole (IDTBT), a high modulus (E \approx 745 MPa) CPs, can be reasonably deformable (crack onset strain [COS] ≈22%). [47] This interesting finding challenges the conventional notion that softness is a prerequisite for achieving deformability in stretchable semiconductive polymers. Similar phenomena have been observed in traditional non-conjugated polymers as well. For instance, polypropylene (PP) with a E of 1360 MPa exhibits a COS of around 180% (true strain), while high-density polyethylene (HDPE) with E of 1050 MPa demonstrates a COS of \approx 200% (true strain). [48] These observations highlight the importance of stretchable rigid polymers for various applications that require robust mechanical properties (e.g., high toughness).[11] Consequently, it is crucial to consider rigid CPs as viable options for deformable materials, as they could become a pivotal component within the stretchable CP family. Despite their potential, the field of stretchable rigid CPs lacks in-depth studies and comprehensive understanding, warranting further research in this area.

The present study aimed to investigate the stretchability of rigid CPs (e.g., E > 700 MPa) in order to explore their molecular origin of high deformability. Mechanical properties of 65 CPs based on different chemical building blocks measured by our group using the "film-on-water" (FOW) characterization technique were organized (chemical structure, molecular weight [MW], elastic modulus (E), and COS are summarized in Table S1, Supporting Information). Surprisingly, 11 CPs showed both high stretchability (COS>20%) and high elastic modulus (>700 MPa), indicating that rigid IDTBT is not the sole example of stretchable rigid CPs. Again, this interesting finding challenges the notion that deformability is directly linked to softness. Subsequently, we conducted a thorough analysis of polymers with the same structure but different MWs and film thicknesses. We found both molecular weight and thickness influenced the mechanical properties by modulating the entanglement behavior of CPs. [49] This led us to deduce that the entanglement effect plays a dominant role in deformability. Furthermore, we systematically investigated the deformation mechanisms and electrical properties of glassy stretchable rigid CPs, focusing on a model polymer, poly(3-butylthiophene-2,5-diyl) (P3BT). This investigation involved multimodal characterization methods, including hard X-ray scattering to probe polymer crystallite, tender X-ray scattering to examine backbone alignment, polarized UV-vis absorption spectroscopy, and coarse-grained molecular dynamics (CG-MD) simulation, for analyzing and understanding polymer chain conformation upon deformation. Notably, we observed different deformation mechanisms between glassy P3BT and a viscoelastic poly(3-octylthiophene-2,5-diyl) (P3OT) sample, primarily characterized by their initial strains. Only the amorphous domains deform at initial stretching (strain<20%) for rigid stretchable CPs, whereas both amorphous and crystallite domains align for normal viscoelastic CPs. After stretching, the mobility increased for both P3BT and P3OT along the parallel direction to stretching. However, in the perpendicular direction, the charge mobility decreased for P3OT at initial strain due to the alignment of the crystallite domain whereas kept constant for P3BT. Such differences did not influence the changed mobility of CPs after stretching. Overall, this work provides new insights into the stretchability of rigid CPs, which can serve as valuable guidelines for the design of rigid stretchable organic semiconductors.

2. Results and Discussion

We initiated our study by examining the mechanical properties of a wide range of CPs including the rigidity (determined by E) and deformability (determined by COS). To accomplish this, we employed a pseudo-free-standing (also known as FOW) tensile test, and the results of 65 CPs, measured by our research group, were organized (Figure 1 and Figure S1-S6 and Table S1, Supporting Information).^[50] The CP thin films were all spin-cast on PSScoated Si wafer followed by flowing on water. The E and COS were calculated based on the stress-strain curve of each CP, which are summarized in Figure 1a. Based on their softness and deformability, we categorized the CPs into four regions: Region I represents brittle rigid CPs, which is similar to "brittle plastics" in polymer science. Region II represents stretchable rigid CPs, similar to "hard plastics." Region III represents brittle soft CPs, similar to "tough plastics," and Region IV represents stretchable soft CPs, similar to "elastomers." The representative stress-strain curves for CPs from each region are shown in Figure 1b. It is evident that multiple CPs are distributed in each region, suggesting that there is no direct correlation between the deformability and softness of CPs. Notably, Region II includes 11 rigid CPs that exhibit substantial deformability, thereby challenging the conventional notion that deformability is exclusively associated with softness. This discovery highlights that stretchability can be achieved by rigid CPs, breaking the stereotype that softness is a prerequisite condition for deformability.[19]

To understand why rigid CPs can exhibit high deformability, we conducted an analysis of CPs with similar structures but varying thicknesses and MWs. Notably, CPs with the same polymer but different MWs and thicknesses demonstrated distinct deformability. In a previous study by Galuska et al., the mechanical properties of poly(naphthalenedimide) (PNDI)-based CPs with MW ranging from 10 to 144 kDa were investigated, revealing the significant influence of MW on deformability, moving the point from Region III to Region IV (COS ranging from ≈2% to over 400%).^[51] We observed similar outcomes in our research. For example, DPPTC2C10C12 with a high MW of 60.6 kDa exhibited a COS ≈16 times higher than that of the 19 kDa counterpart, also moving the point from Region III to Region IV (Figure S2 and Table S1, Supporting Information). Besides, Zhang et al. measured the mechanical property of poly(3-hexylthiophene) (P3HT) with a thickness of \approx 20–95 nm. ^[52] The COS increased first with increasing thickness and then decreased for films thicker than 80 nm. The decreased COS in thin films was attributed to the reduced interchain entanglements in this film, whereas the decreased COS of the thicker film was attributed to the presence of more defects that can initiate and propagate the cracks. Both MW and thickness have an effect on the entanglement of CP chains. [49] Based on these observations, we deduced that chain entanglement is a critical factor governing the deformability of CPs, which is consistent with previous reports by the Lipomi

16163028, 0, Downloaded from https://onlinelibrary.wiley.com/doi/10.1002/adfm.202306576 by Univ of California Lawrence Berkeley National Lab, Wiley Online Library on [28/11/2023]. See the Terms and Conditions (https://onlinelibrary.wiley.com/doi/10.1002/adfm.202306576 by Univ of California Lawrence Berkeley National Lab, Wiley Online Library on [28/11/2023]. See the Terms and Conditions (https://onlinelibrary.wiley.com/doi/10.1002/adfm.202306576 by Univ of California Lawrence Berkeley National Lab, Wiley Online Library on [28/11/2023]. See the Terms and Conditions (https://onlinelibrary.wiley.com/doi/10.1002/adfm.202306576 by Univ of California Lawrence Berkeley National Lab, Wiley Online Library on [28/11/2023]. See the Terms and Conditions (https://onlinelibrary.wiley.com/doi/10.1002/adfm.202306576 by Univ of California Lawrence Berkeley National Lab, Wiley Online Library on [28/11/2023]. See the Terms and Conditions (https://onlinelibrary.wiley.com/doi/10.1002/adfm.202306576 by Univ of California Lawrence Berkeley National Lab, Wiley Online Library on [28/11/2023]. See the Terms and Conditions (https://onlinelibrary.wiley.com/doi/10.1002/adfm.202306576 by Univ of California Lawrence Berkeley National Lab, Wiley Online Library on [28/11/2023]. See the Terms and Conditions (https://onlinelibrary.wiley.com/doi/10.1002/adfm.202306576 by Univ of California Lab, Wiley Online Library on [28/11/2023]. See the Terms and California Lab, Wiley Online Library on [28/11/2023]. See the Terms and California Lab, Wiley Online Library on [28/11/2023]. See the Terms and California Lab, Wiley Online Library on [28/11/2023]. See the Terms and California Lab, Wiley Online Library on [28/11/2023]. See the Terms and California Lab, Wiley Online Lab, Wiley Online Library on [28/11/2023]. See the Terms and California Lab, Wiley Online Lab

on Wiley Online Library for rules of use; OA articles are governed by the applicable Creative Commons

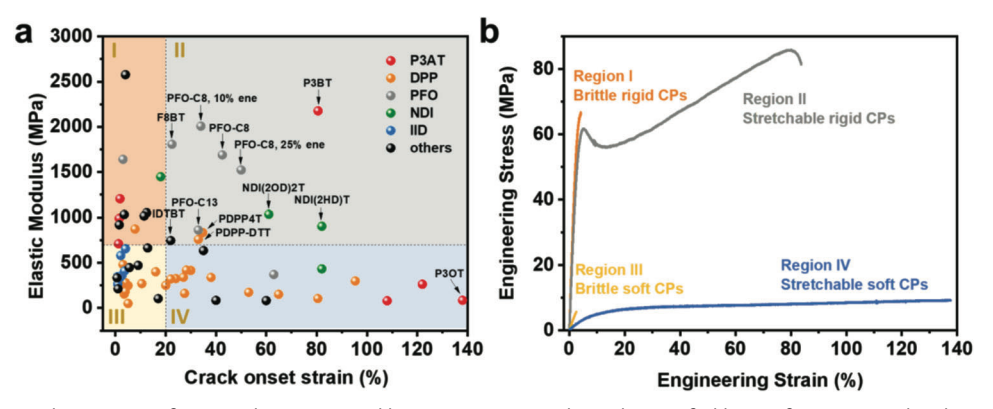


Figure 1. The mechanical properties of 65 samples were tested here. a) Summarized E and COS of a library of CPs surveyed in this work. Region I: Rigid and brittle CPs with high E and low COS. Region II: Rigid and deformable CPs with high E and high COS. Region III: Soft and brittle CPs with low E and low COS. Region IV: Soft and deformable CPs with low E and high COS. b) Representative stress—strain curve for polymers from each region. Representative material for Region I: PCPDTBT (MW: 17.8 kDa, thickness: 76 nm), Region II: P3BT (MW: \approx 60 kDa, thickness: 46 nm), Region III: DPPTTC2C10C12 (MW: 29.0 kDa, thickness: 82 nm), Region IV: P3OT (MW: \approx 80 kDa, thickness: 53 nm).

group and the Kim group.^[53,54] Rigid CPs with higher chain entanglement can still exhibit deformability.

We proceeded to investigate the mechanical behavior, the influence of rigidity on electrical properties, and the deformation mechanism of deformable rigid CPs using a representative pair of model CPs: a glassy rigid P3BT and a viscoelastic soft P3OT (Figure 2a). These model CPs share a similar structure, molecular weight, and thickness, differing only in their side-chain lengths. The rigidity of P3BT stems from its restricted chain mobility, attributed to its glassy state at room temperature ($T_{\rm g}=52$ °C) (Figure S7 and Table S2, Supporting Information). In contrast, the lower elastic modulus (*E*) of P3OT is a consequence of its lower $T_{\rm g}$ (–13 °C), achieved through the incorporation of longer alkyl side chains (Figure S7 and Table S2, Supporting Information).

The mechanical behavior of P3BT and P3OT was first studied. True stress–true strain $(\sigma_{\rm T}-\epsilon_{\rm T})$ curve was used to describe the mechanical properties. The true strain takes into account the in-

stantaneous and local changes in the material's dimensions as it deforms.^[55] It provides a more accurate measure of strain when the material undergoes plastic deformation. True stress was calculated using the equation $\sigma_T = \sigma(1 + \epsilon)$, where σ is the engineering stress, ϵ is the engineering strain. True strain was calculated using the equation, $\epsilon_{\rm T} = \ln(1 + \epsilon)$. The true stress-true strain $(\sigma_T - \epsilon_T)$ curves for both CPs are shown in Figure 2b. P3BT showed a significantly higher *E* of 2216 MPa compared to P3OT (86 MPa) due to the limited chain mobility in its glassy state. [56] Despite the \approx 30-fold difference in *E*, both CPs displayed high COS of $\epsilon_{\rm T}$ \approx 60–80%. The entanglement molecular weight for P3BT and P3OT were reported to be 4.1 and 5.6 kg mol⁻¹, respectively.^[57] Based on the entanglement molecular weight, the average number of entanglements per polymer chain was estimated to be 14.6 and 14.3 for P3BT and P3OT. The weight average molecular weight of P3BT and P3OT we used in this work is ≈60 and ≈80 kDa, which were much higher than their entanglement molecular weight. Therefore, they both performed high

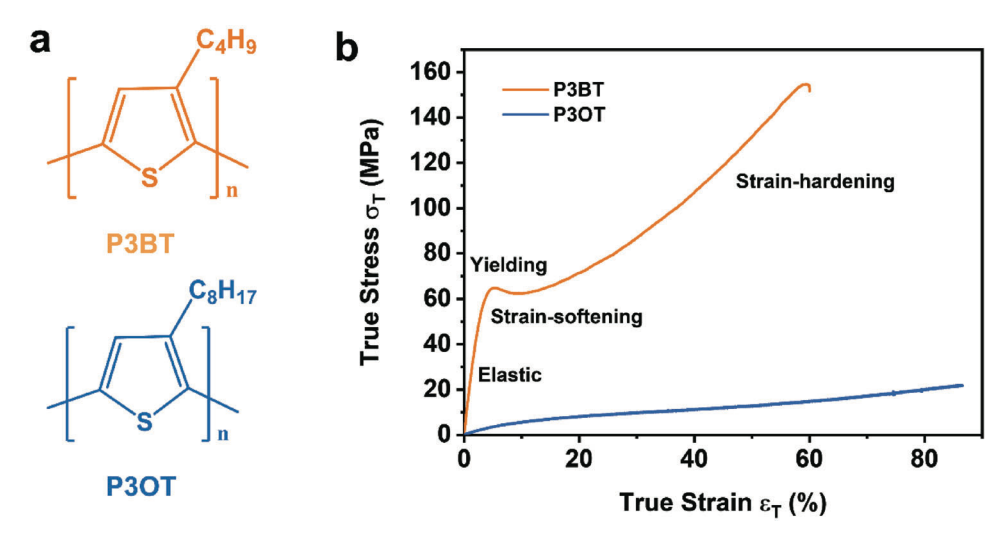


Figure 2. a) Molecular structure and b) true stress-strain curves for P3BT and P3OT thin films. Note the distinct mechanical response from glassy P3BT and viscoelastic P3OT systems.

16 16 3028, 0, Downloaded from https://onlinelibrary.wiley.com/doi/10.1002/adfm.202306576 by Univ of California Lawrence Berkeley National Lab, Wiley Online Library on [28/11/2023]. See the Terms and Conditions (https://onlinelibrary.wiley

use; OA articles are governed by the applicable Creative Commons

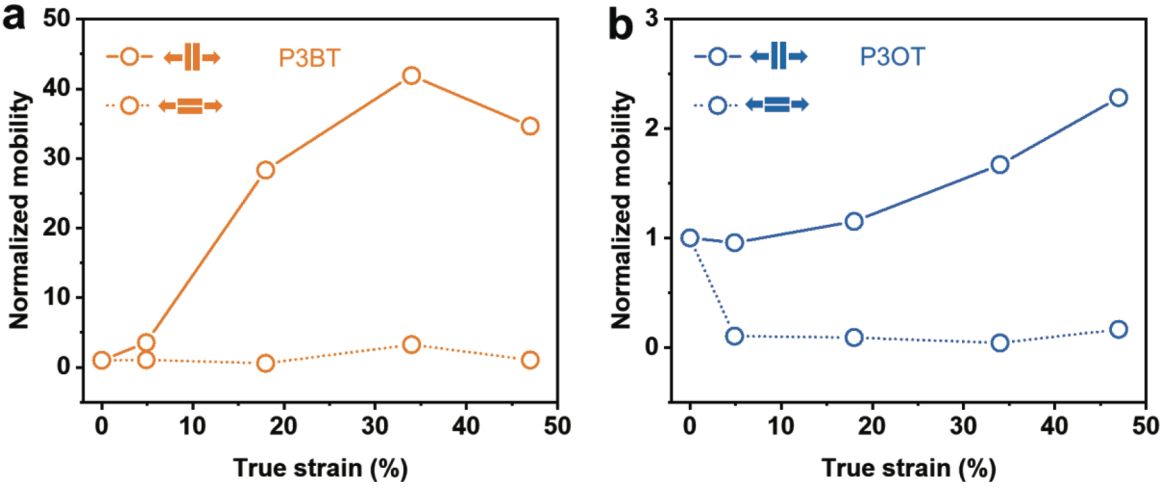


Figure 3. Normalized transistor mobility of stretched a) P3BT and b) P3OT at different degrees of strain. The value of the charge carrier mobility is listed in Table 1, obtained from an organic thin film transistor setup.

deformability. However, distinct mechanical behaviors were observed between P3BT and P3OT. Four regions were observed for P3BT from the $\sigma_{\rm T}$ – $\epsilon_{\rm T}$ curve, including a linear elastic region $(\epsilon_{\rm T}=0$ –3%), a well-defined mechanical yielding ($\epsilon_{\rm T}=$ 5%), a strain-softening ($\epsilon_T = 5$ –9%) and strain hardening region (ϵ_T > 9%), which were similar to the previous report.^[58] In contrast, P3OT lacked a clear yielding point and strain-softening region. Traditional semicrystalline polymers with a high degree of crystallinity, such as PE, typically exhibit yielding and strain-softening mechanisms associated with crystallographic deformations and necking. [48,59] However, P3BT did not show necking behavior. The yielding and strain-softening observed in P3BT originated from amorphous chain deformations, as supported by the subsequent morphology study, distinguishing it from PE. Strain-hardening is typical for CPs. Previous findings from our group demonstrated that the slope of the strain-hardening region decreases with increasing side-chain length, which is consistent with the behavior observed in P3BT and P3OT.[37]

The effect of glassiness on the electrical properties of strainaligned CPs is then studied by fabricating top-contact bottomgate organic field-effect transistors (OFETs). To highlight the local alignment and charge transport anisotropy, we utilized a small channel length of 10 µm, a method previously employed to measure the anisotropy of charge mobility for poly(3-alkylthiophene) P3AT CPs. [60] Results are summarized in Figure 3, Table 1, and Tables S3,S4, Supporting Information. Transfer curves are shown in Figure S8-S11, Supporting Information. We measured the charge mobility along both the parallel and perpendicular directions to the stretching, aiming to study the anisotropy in charge carrier mobility under deformation. Along the direction parallel to the strain, the charge mobility for both P3BT and P3OT remained relatively constant within the elastic region, as only the amorphous components were aligned. Subsequently, a significant increase in charge mobility was observed due to the alignment of the crystallite domains. Conversely, along the perpendicular direction, the charge mobility decreased for P3OT, similar

Table 1. Summary of the OFETs performance of stretched P3BT and P3OT thin films.

ε _T [%] ^{a)}		P3BT		РЗОТ			
	$\mu_{\text{ave}}^{\text{ b)}} [\text{cm}^2 \text{ V}^{-1} \text{ S}^{-1}]$	$I_{\rm on}/I_{\rm off}$	V_{th}	$\mu_{\text{ave}}^{\text{ b)}} \text{ [cm}^2 \text{ V}^{-1} \text{ S}^{-1}]$	I _{on} /I _{off}	V_{th}	
0	9.5 × 10 ⁻⁶	1.6 × 10 ¹	7.9	3.5×10^{-3}	6.8 × 10 ³	-10.6	
5	3.4×10^{-5}	1.3×10^{2}	-24.5	3.4×10^{-3}	2.6×10^{3}	-14.7	
5 ⊥	1.8×10^{-5}	3.1×10^{2}	-14.9	6.7×10^{-4}	4.1×10^{2}	-7.8	
18	2.7×10^{-4}	6.8×10^{2}	-15.8	4×10^{-3}	6.2×10^{3}	-12.2	
18 ⊥	7.9×10^{-6}	3.8×10^{1}	-25.1	4.5×10^{-4}	3.8×10^{2}	-4.9	
34	4×10^{-4}	1.2×10^{2}	-12.5	5.9×10^{-3}	6.2×10^{3}	-11.3	
34 ⊥	7.4×10^{-5}	3.2×10^{2}	-17.4	3.3×10^{-4}	5.8×10^{2}	2.7	
47	3.3×10^{-4}	1.3×10^{2}	-10	8.0×10^{-3}	5.5×10^{3}	-10	
47 ⊥	1.3×10^{-5}	1.7×10^{1}	3.8	3.2×10^{-4}	1.6×10^{2}	-3.4	

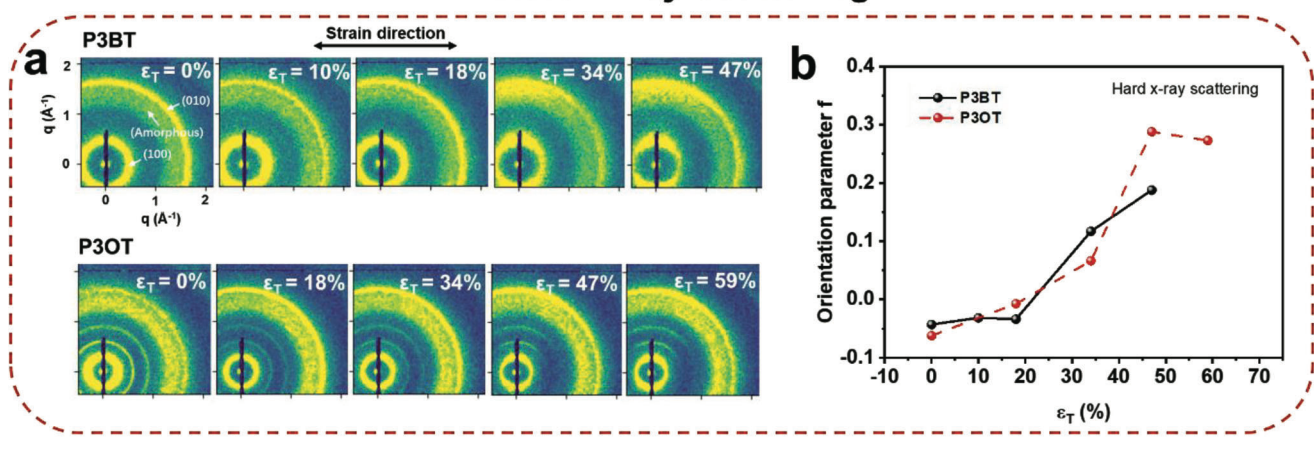
a) The applied strains and channel directions parallel (||) and perpendicular (⊥) to the applied strains; b) The calculated electron mobility of the devices averaged from five devices within three batches.

16163028, 0, Downloaded from https://onlinelibrary

wiley.com/doi/10.1002/adfm.202306576 by Univ of California Lawrence Berkeley National Lab, Wiley Online Library on [28/11/2023]. See the Terms.

on Wiley Online Library for rules of use; OA articles are governed by the applicable Creative Common

Hard X-ray scattering



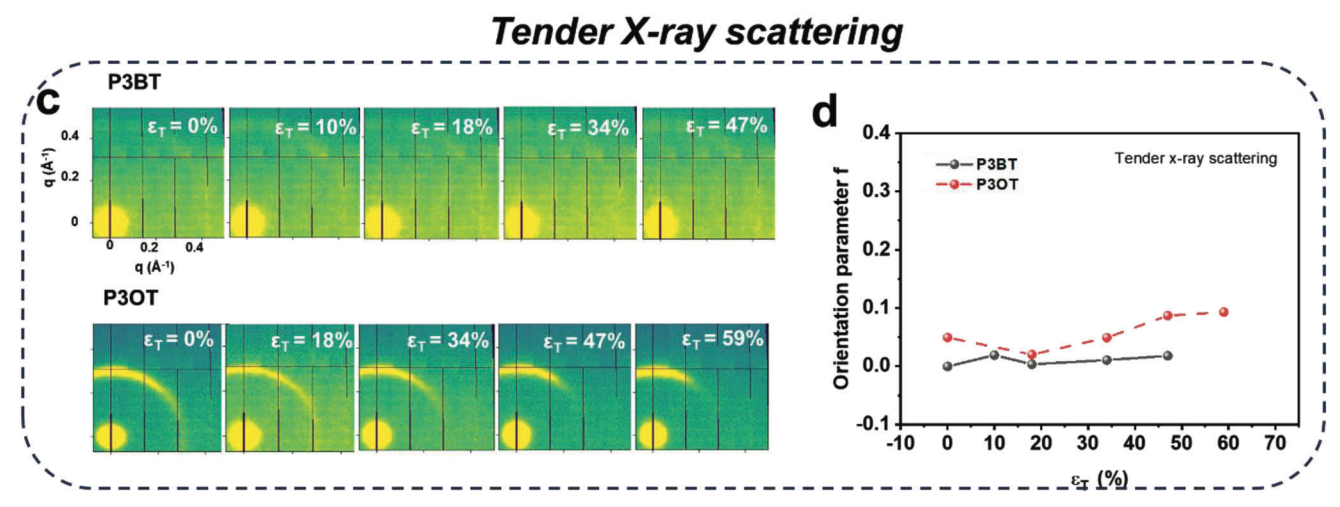


Figure 4. Experimental result for hard/tender WAXS experiment on P3BT and P3OT polymer thin films under various true strains. Representative 2D scattering patterns and characteristic crystallographic peaks of P3BT and P3OT from a) hard and c) tender WAXS. Herman's orientation parameter f versus strain based on (100) peak of P3BT and P3OT from b) hard and d) tender WAXS.

to the previously reported behavior for P3HT,[61] but remained nearly constant for P3BT. This discrepancy can be attributed to the frozen nature of the chains in P3BT, which hinders their alignment. Moreover, the charge transport along the polymer main chain exhibited significantly better performance compared to the π – π intermolecular transport. The intricate mechanism behind chain alignment will be further investigated in the subsequent section. The changes in charge transport did not exhibit significant differences between rigid and soft stretchable CPs, highlighting the substantial potential of rigid stretchable CPs for future applications. The threshold voltage was found to be overall similar for both P3BT and P3OT. However, the on/off ratio of P3BT was observed to be lower compared to P3OT. This difference can be attributed to the higher homo energy level of P3BT, which makes it more sensitive to the doping effect caused by oxygen/water.[62-64]

The deformation mechanism difference between glassy P3BT and viscoelastic P3OT was then investigated using a comprehensive set of characterization methods to fully understand the device performance. The detailed procedure for sample preparation can be found in the Supporting Information. In summary, thin

films of stretched CPs with a thickness of ≈60 nm were subjected to stretching using a pseudo-free-standing tensile tester. Subsequently, these strained free-standing films were transferred onto a washer's frame to facilitate further characterization (Figure S12a, Supporting Information).

Wide-angle hard X-ray scattering (Hard WAXS) was conducted to investigate the alignment of crystallite domains.^[65] The measurements were performed in transmission geometry, with the X-ray beam perpendicular to the sample plane. The samples were mounted in a manner that aligned the stretching direction horizontally with the polarization direction of the beam (Figure S12b, Supporting Information). As a result, the equatorial and meridian directions corresponded to the parallel and perpendicular directions to the stretching axis, respectively. Detailed information about the characterization methods can be found in the Supporting Information. The 2D scattering patterns of the samples under different strain conditions are shown in Figure 4a, accompanied by the corresponding 1D scattering profiles and pole figures shown in Figure S13,S14, Supporting Information. The results were processed using Python code according to a previous literature

16163028, 0, Downloaded from https://onlinelibrary

wiley.com/doi/10.1002/adft.20.2306576 by Univ of California Lawrence Berkeley National Lab, Wiley Online Library on [28/11/2023]. See the Terms and Conditions (https://onlinelibrary.wiley.com/terms-and-conditions) on Wiley Online Library for rules of use; OA articles are governed by the applicable Creative Commons

Table 2. Crystallographic information for P3BT and P3OT extracted from wide-angle hard X-ray scattering.

	ϵ_{7}	Equatorial direction				Meridian direction			
		(100)			(010)	(100)			(010)
		(100) peak <i>q</i> [Å ⁻¹]	FWHM [Å ⁻¹]	τ [Å]	– (010) peak <i>q</i> [Å ⁻¹]	(100) peak <i>q</i> [Å ⁻¹]	FWHM [Å ⁻¹]	τ [Å]	(010) peak <i>q</i> [Å ⁻¹]
P3BT	0	0.47	0.10	7.7	1.65	0.47	0.10	7.98	1.64
	10%	0.47	0.10	7.3	1.65	0.47	0.10	7.93	1.65
	18%	0.47	0.11	7.1	1.64	0.47	0.11	7.27	1.62
	34%	0.49	0.25	3.2	1.67	0.47	0.10	7.48	1.63
	47%	0.48	0.23	3.5	1.66	0.47	0.12	6.49	1.65
P3OT	0	0.30	0.04	17.1	1.66	0.30	0.04	17.3	1.65
	18%	0.30	0.04	17.4	1.63	0.30	0.04	17.3	1.64
	34%	0.30	0.04	17.2	1.64	0.30	0.04	17.3	1.64
	47%	0.30	0.07	10.8	1.65	0.30	0.04	17.3	1.64
	59%	0.30	0.06	12.6	1.65	0.30	0.04	17.3	1.63

The coherence length τ is calculated by the Scherrer equation: $\tau = (K \times \lambda)/(\beta \times \cos \theta)$, where K = 0.9, $\lambda = 0.77$ Å for X-ray energy of 16.1 keV, β is the FWHM, and θ is the Bragg angle.

report.[66] Key parameters including peak position (q), full width at half maximum (FWHM), and coherence length (τ) extracted from the WAXS measurements are summarized in Table 2. Three representative peaks can be observed on the 2D patterns as illustrated in Figure 4a: the lamellae packing peak (100), the π - π stacking peak (010), and an amorphous halo. P3BT showed a smaller lamellar packing distance (13.4 Å) compared to P3OT (20.9 Å) due to its shorter side chain. Upon stretching, the peak position of the (100) peak for both polymers showed only a slight change, indicating an unchanged packing distance. For P3BT, the (100) peak was stated to exhibit anisotropy at $\epsilon_T = 34\%$, signifying the initiation of crystallite orientation/rotation. Concurrently, the coherence length along the equatorial direction experienced a significant decrease from $\epsilon_{\rm T}$ = 34%, indicating the deformation of crystallite domain parallel to the strain direction. In contrast, for P3OT, the (100) peak began to exhibit anisotropy at an earlier strain of ϵ_T = 18%, while the coherence length started to decrease from $\epsilon_{\rm T}$ = 47%, suggesting the initiation of crystallite rotation at the smaller strain but large deformation occurring at $\epsilon_T = 47\%$.

2D Herman's orientation parameter f for the (100) peak was then calculated based on the pole figures (Figure S14, Supporting Information) to quantify the degree of alignment, following the method described in a previous report (Figure 4b).[37] The values of f for P3BT and P3OT started to increase at $\epsilon_{\rm T}$ = 34% and $\epsilon_{\rm T}$ = 18%, respectively, which aligned well with the observations from the 2D images shown. At $\epsilon_T = 0.47$, fincreased by 0.23 for P3BT but 0.34 for P3OT. The larger increase in f for P3OT indicates a higher degree of alignment of the crystalline domain, attributed to the greater chain flexibility of the viscoelastic polymer. Smallangle hard X-ray scattering (SAXS) was also performed to investigate the crystallite distance (Figure S15, Supporting Information). However, no peak was observed, probably due to a low degree of crystallinity. As a result, the spacing between crystals falls outside the q range probed by the measurement, similar to previous observations for DPP-based donor-acceptor polymers.[37] The alignment of the π – π stacking peak and the amorphous halo is discussed in Figure S16, Supporting Information. Based on the findings from hard X-ray scattering, we can conclude that there is no crystallite domain alignment for P3BT at initial strain, whereas crystalline rotation contributes to the strain at first and crystallite deformation joins after $\epsilon_{\rm T}$ = 47% for P3OT. Additionally, we performed in situ hard WAXS to stretch CP films under the same beamline (Figure S17–S20, Supporting Information). The peak position almost kept constant upon stretching, indicating the film relaxation did not influence the study of the deformation mechanism (Figure S18e,f, Supporting Information). However, FWHM did not change at the strain of 50% either, which was different from the ex situ experiment. We attributed this difference to the variation in the thickness of the materials, which was thin-film for ex situ experiment and bulk for in situ experiment. The crystallite structure under a thin-film state was easier to break due to less entanglement.

Wide-angle tender X-ray scattering (tender WAXS) was conducted using X-ray energy near the sulfur K-edge (≈2.47 keV) to specifically detect the backbone orientation in the crystalline regions of the CPs. [37,67-69] The backbones of CPs are crucial for charge transport due to the conjugated structure. Given the inherent difference in rigidity between the backbone and sidechain of CPs, we hypothesize that there may be distinct alignment behaviors between the backbone and the entire polymer chains. As the energy was scanned across the sulfur K-edge (2.46–2.5 keV), scattering patterns were recorded. The background intensity variation at different energies, shown in Figure S21, Supporting Information, originates from the fluorescence of sulfur atoms. The fluorescence signal exhibits a plateau below 2.47 keV and a sharp increase for both polymers at 2.476 keV. The maximum of the fluorescence signal was reached at 2.478 keV, which is usually close to the energy where the sulfur atoms contribute optimally to the scattering signal. Characteristic 2D scattering patterns and corresponding 1D plots along equatorial and meridian directions under an X-ray energy of 2.478 keV are shown in Figure 4c and Figure S22-S26, Supporting Information. Due to the restricted

1616:3028, 0, Downloaded from https://onlinelibrary.wiley.com/doi/10.1002/adfm.202306576 by Univ of California Lawrence Berkeley National Lab, Wiley Online Library on [28/11/2023]. See the Terms and Conditions (https://onlinelibrary.wiley

conditions) on Wiley Online Library for rules of use; OA articles are governed by the applicable Creative Commons

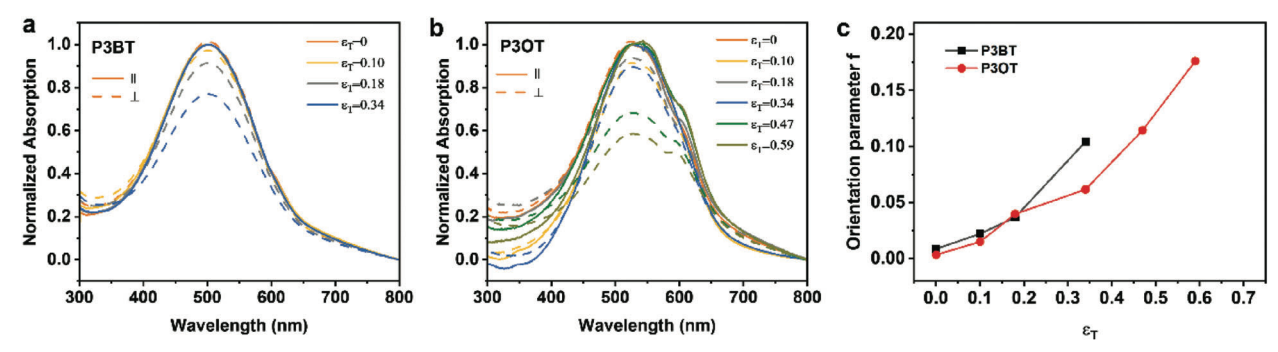


Figure 5. Whole chain alignment study from polarized UV–vis spectroscopy. UV–vis absorption plot at different wavelengths for a) P3BT and b) P3OT under various strains. c) Herman's orientation parameter *f* under strain.

high q range accessible with tender X-ray, only the (100) peak could be easily measured in this work. The fluorescence of sulfur was too strong as the background at the sulfur K-edge (≈2478 eV), which hindered the lamellar peak. Consistent with the findings from hard X-ray scattering, P3BT exhibited higher q values for lamellae packing peak and a shorter packing distance compared to P3OT, attributable to its shorter side chains. Similar to the hard X-ray analysis, Herman's orientation parameter *f* at five energies from 2.470 to 2.478 keV was obtained from pole figures (Figure S25,S26, Supporting Information) of both polymers, as summarized in Figure 4d and Figure S27, Supporting Information. The f value obtained at 2.470 keV, away from the edge, closely matched the value extracted from the hard X-ray scattering experiments, as no resonant effect was present. From 2.470 to 2.474 keV, the f value gradually decreased. At 2.478 keV, the backbone orientation signal predominated. For P3BT, f remained almost unchanged upon stretching, suggesting the absence of backbone orientation in the crystallites. Conversely, for P3OT, a slight increase in f indicated less pronounced chain slippage behavior, consistent with our previous findings for low- T_{α} DPP-based CPs.^[37] Consequently, while noticeable backbone alignment in the crystalline regions was observed in viscoelastic CPs, it was limited in glassy CPs. For both P3BT and P3OT, fs from tender X-ray scattering are much lower than those from hard X-ray scattering, indicating the backbone orientation is smaller than the whole chain orientation due to the limited mobility of conjugated structures.

Polarized UV–vis was used to study the overall polymer backbone alignment combining crystallite region and amorphous chain. This technique enables the examination of the combined alignment of the crystalline regions and amorphous chains when the transition dipole moment (π – π *) is parallel to the long axis of the polymer backbone.^[70] The normalized absorption spectrum of strained P3BT and P3OT thin films under strain are plotted in **Figure 5**a and Figure 5b, respectively. The 0 \rightarrow 0 and 0 \rightarrow 1 transition occurred at \approx 591 and \approx 499 nm, respectively. 0-0 absorption peak was favorable along the strain direction, attributed to polymer long-axis alignment.^[61] To quantify the anisotropy, the dichroic ratio, R, was calculated using the following equation

$$R = \frac{A_{\parallel}}{A_{\perp}} \tag{1}$$

where A_{\parallel} and A_{\perp} is the 0-0 peak absorbance of the film with polarized light parallel and perpendicular to the strain direction, re-

spectively. Then, Herman's orientation parameter f can be determined

$$f = \frac{R-1}{R+1} \tag{2}$$

Surprisingly, Herman's orientation parameter, f, exhibited similar behavior for both P3BT and P3OT, suggesting that the T_{α} did not significantly affect the alignment of the entire polymer chain during stretching (Figure 5c). Notably, f showed a gradual increase throughout the stretching process, albeit to a limited extent. This trend aligns with our previous findings in DPPbased polymers, [37] indicating that polymer chain alignment occurs throughout the deformation process but with relatively low anisotropy. In the case of P3BT, where crystallite alignment was initially limited, the alignment of the amorphous chains played a significant role in the initial deformation (ϵ_T < 0.18). On the other hand, P3OT exhibited a distinction between crystallite and overall chain alignment, suggesting that both crystalline and amorphous regions contributed to the deformation process. Therefore, the limitation in alignment was primarily observed in the crystallite domain for glassy CPs. Additionally, we also investigated polarized UV-vis spectroscopy for samples supported by PDMS, and the results are presented in Figure S28, Supporting Information. For more details, please refer to the Supporting Information.

In addition to the experimental investigations, we utilized CG-MD simulation to gain further insights into the impact of measurement temperature on the mechanical behaviors and chain alignment upon thin-film deformation (Figure 6 and Figure S29-S32, Supporting Information). Our CG model utilized a "beadspring" representation of the polymer, incorporating a branched chain structure to capture the essential structural characteristics of CPs. Specifically, the CG model consisted of a linear backbone chain (represented by pink beads), with each backbone bead connected to an alkyl side chain (represented by blue beads) to simulate the alkyl groups (Figure 6a). Figure 6b shows a snapshot of free-standing thin film simulations using the CG model. The effect of side-chain length on thermomechanical behavior was first simulated, which is discussed in detail in Supporting Information. The result agreed reasonably well with experimental data. The orientation of polymer chains was evaluated by calculating the orientation parameter f of the thin film system^[37,71]

$$f = \left\langle \frac{3}{2} \cos^2 \theta - \frac{1}{2} \right\rangle \tag{3}$$

16 16 3028, 0, Downloaded from https://onlinelibrary.wiley.com/doi/10.1002/adfm.202306576 by Univ of California Lawrence Berkeley National Lab, Wiley Online Library on [28/11/2023]. See the Terms and Conditions (https://onlinelibrary.wiley

and-conditions) on Wiley Online Library for rules of use; OA articles are governed by the applicable Creative Commons

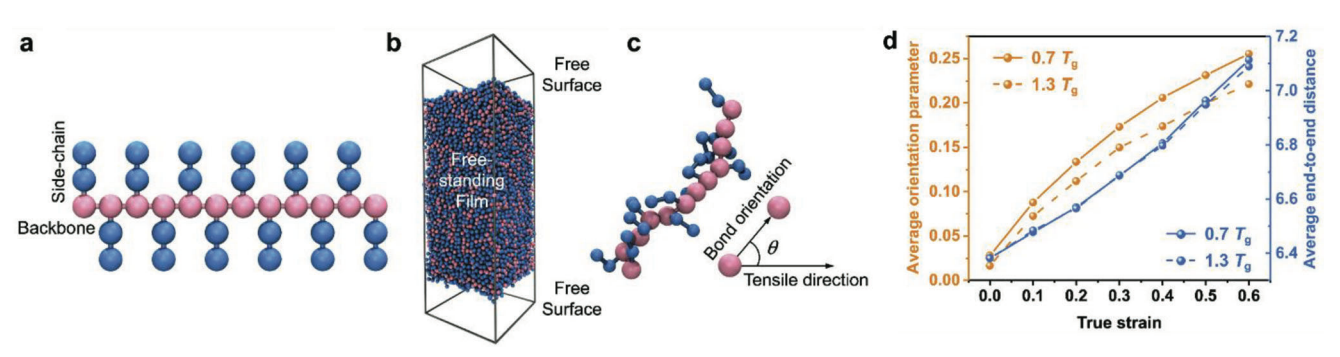


Figure 6. Amorphous component alignment study from CG-MD simulation. a) Schematic illustration of CG polymer model with branched side-chain. b) Snapshot of the CG free-standing thin film. c) Schematic of a single polymer chain with a defined angle between the bond orientation and tensile direction. d) Average orientation parameter (left y-axis) and end-to-end distance (right y-axis) versus strain for two representative T.

where θ is the angle formed by the bond vector connecting two consecutive backbone CG beads relative to the deformation direction, and the bracket denotes the ensemble average over all bond vectors (Figure 6c). Furthermore, we calculated the end-to-end distance of the polymer backbone to gain a deeper understanding of the chain orientation. Figure 6d shows clear evidence that, as the tensile strain increased, the polymer chains exhibited a greater tendency to align along the deformation axis, resulting in a higher orientation parameter, accompanied by the increase in the end-to-end distance of the polymer chains. To explore the local orientation distribution, we further generalized Equation (3) to evaluate the local orientation parameter based on individual bond vectors in the thin film system. The probability distributions of local orientation parameters upon deformation for different *T* are presented in Figure S31a, Supporting Information. In all cases, a Gaussian-like distribution was observed, with the peak gradually decreasing and shifting toward higher values, indicating a propensity for backbone orientation in the direction of strain. A similar trend was observed for the end-to-end distance distribution, as shown in Figure S31c, Supporting Information. It is worth noting that both *f* value and end-to-end distance at each strain were nearly independent of temperature (Figure S30,S31b,d, Supporting Information), which was also consistent with the above experimental observation that the T_a of CPs did not show direct influence on the chain alignment under strain. This observation aligns with the experimental finding, indicating that the T_g of CPs does not directly influence entire chain alignment under strain.

By combining the findings from both experiments and simulations, we can elucidate the deformation mechanisms of glassy P3BT and viscoelastic P3OT. In the case of glassy P3BT, during the initial stage of deformation ($\epsilon_{\rm T} < 0.18$), only the orientation of the amorphous chains contributed to the overall deformation process. Subsequently, the crystalline domains experienced breaking, rotation, and alignment, as evidenced by the decreased coherent length and increased orientation parameter (f) values for the lamellar stacking peak, π – π stacking peak, and amorphous halo. The amorphous domain within P3BT serves as tie chains (bridging chains) between crystallite domains. It is reported that the high content of tie chains in the amorphous domain plays a crucial role in facilitating charge transport due to the difficulty of charge transport between ordered regions. [72] There-

fore, with amorphous domains alignment within $\epsilon_{\rm T}$ < 0.18, the charge mobility increased. Upon further stretching, the crystallite domain begins to align resulting in higher charge mobility. In contrast, for the viscoelastic polymer P3OT, both the alignment of lamellar structures and the amorphous chains played significant roles throughout the entire deformation strains. The alignment of crystals is known to facilitate charge transport along the direction parallel to the stretching direction, whereas crystal deformation can sometimes have a negative impact on charge mobility.[61] In the case of P3OT, both crystal alignment and crystal deformation occur. Interestingly, the charge mobility continues to increase in a parallel direction but decreases in a perpendicular direction indicating crystal alignment somehow overcompensates for the crystal disruption in P3OT. In a previous study, the Salleo Group found that short-range intermolecular aggregation is sufficient for charge transport. [73] Based on this understanding, we deduce that the deformed crystals are still large enough to support charge transport. This behavior is consistent with what has been observed in viscoelastic DPP-based polymers previously studied.[37]

To verify the universality of our observations, we selected poly(9,9-dioctylfluorene-alt-benzothiadiazole) (F8BT) as another deformable glassy CP with a high T_o of 111.6 °C (Figure 7a). The stress-strain behavior of F8BT is shown in Figure 7b, with a critical strain (COS) of ≈20% and a similar high elastic modulus of 1807 MPa compared to P3BT. The same morphology characterization methods were used for F8BT. However, unlike P3BT, F8BT did not show the 0-0 aggregation peak at 540 nm in UV-vis spectra as reported.^[74] Therefore, we focused on evaluating the chain alignment mechanism of F8BT using wide-angle hard/tender Xray scattering. The results are shown in Figure 7c and Figure S33-S39 and Table S5, Supporting Information. We found the thin film broke without any crystallite alignment and deformation for F8BT, resembling the initial deformation region observed in P3BT. The earlier breakage in F8BT may be attributed to the difficulty in aligning the crystalline region, primarily influenced by intra/inter-crystallite interaction strength and a reduction in the number of entanglements/tie-chains. It is important to note that if there is a sufficient amorphous domain allowing for the rotation of crystallite domains, rigid CPs can exhibit stretchability. However, if the amorphous domain is insufficient, the CPs tend to be brittle.

16163028, 0, Downloaded from https://onlinelibrary.wiley.com/doi/10.1002/adfm.202306576 by Univ of California Lawrence Berkeley National Lab, Wiley Online Library on [28/11/2023]. See the Terms

on Wiley Online Library for rules of use; OA articles are governed by the applicable Creative Commons

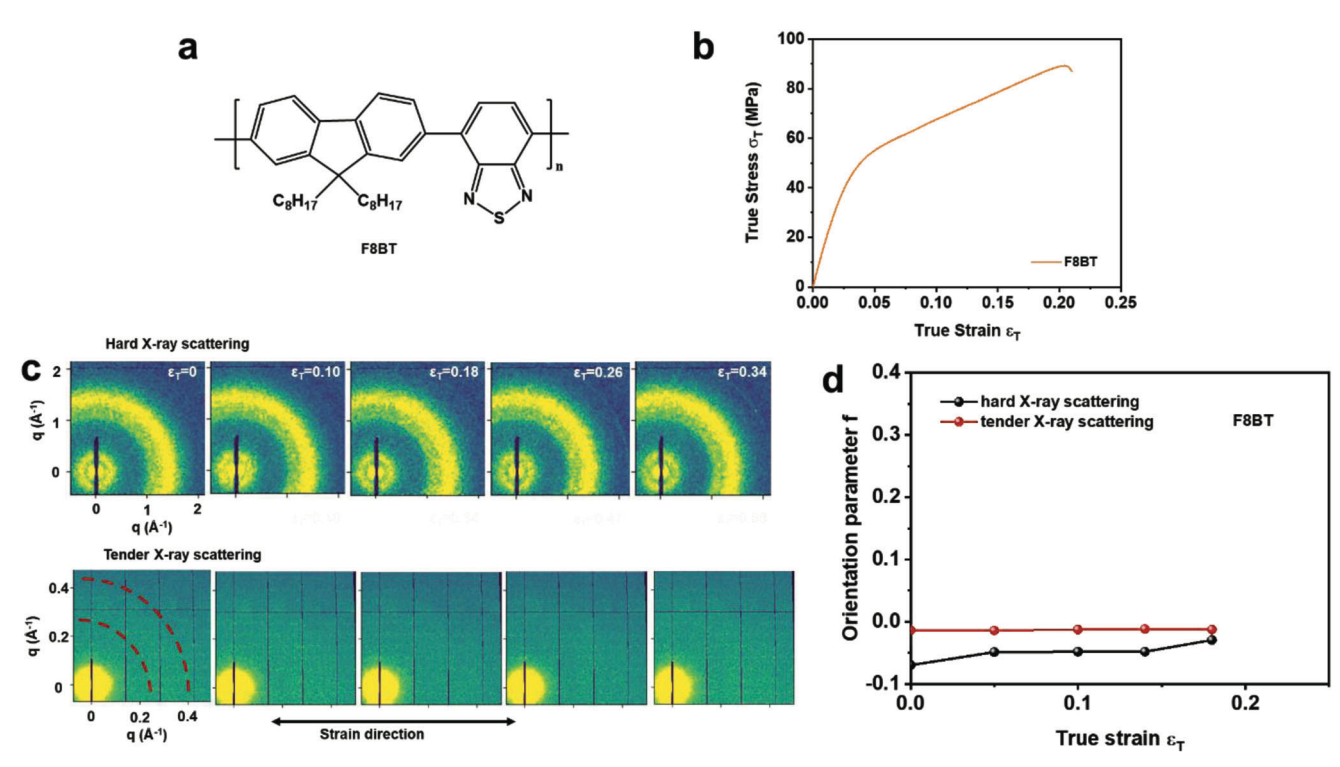


Figure 7. a) Molecular structure for glassy F8BT. b) True stress–strain curves for F8BT. c) Representative 2D scattering patterns and characteristic crystallographic peaks of F8BT from hard and tender WAXS. d) Herman's orientation parameter f versus strain based on (100) peak of F8BT from hard and tender WAXS.

3. Conclusion

Our study focused on the mechanical performance of 65 different CPs with the aim of assessing their suitability for stretchable electronics applications. Contrary to common assumptions, we discovered that the rigidity of a CP does not necessarily determine its deformability. In fact, our results suggest that even rigid, glassy CPs exhibit promising characteristics for stretchable electronics. To gain deeper insights into the mechanical behavior, electrical properties, and chain alignment mechanisms of these unique glassy CPs, we conducted a comprehensive analysis focused on a model CP called P3BT, as well as its viscoelastic counterpart, P3OT. Our investigation revealed an intriguing feature in P3BT, namely an additional yielding and strain-softening region compared to P3OT. Remarkably, this difference did not significantly impact the charge mobility of the stretched CPs. By employing a combination of wide-angle hard/tender X-ray scattering, polarized UV-vis, and CG-MD simulation techniques, we scrutinized the chain alignment mechanism of these CPs. The results uncovered a key disparity between P3BT and P3OT, primarily in their initial strain behavior. In the case of P3BT, the deformation was predominantly facilitated by the slipping of amorphous domains, attributed to its frozen chain nature at room temperature, for the first 18% strain. In contrast, both amorphous chain and crystallite rotation played a role in the deformation of P3OT. Overall, our study provides a comprehensive understanding of the stretchability of glassy CPs and challenges the conventional notion that only flexible CPs are suitable for wearable electronics. These findings underscore the great potential of even rigid CPs in the realm of wearable electronics and offer valuable insights for the design and development of future stretchable electronic devices.

Supporting Information

Supporting Information is available from the Wiley Online Library or from the author.

Acknowledgements

Y.W. and S.Z. contributed equally to this work. Y.W. and X.G. thanks the financial aid from NSF grant DMR-2047689 for supporting the majority of this work, particularly the mechanical characterization. Y.W. was supported in part by an ALS Doctoral Fellowship in Residence. Z.C. and X.G. thank the Department of Energy for supporting the X-ray scattering of this work under grant number DE-SC0022050. This research used resources beamline 12-ID of the National Synchrotron Light Source II, a U.S. Department of Energy (DOE) Office of Science User Facility operated for the DOE Office of Science by Brookhaven National Laboratory under Contract No. DE-SC0012704. The authors thank Mikhail Zhernenkov (NSLS-II) for his assistance at the beamline and for the helpful discussions. S.Z. thanks NSF OIA-1757220 for supporting his work. Z.L. and W.X. acknowledge the support from NSF OIA-2119691 (AI-SUSTEIN). Access to the CCAST supercomputing capability at NDSU is also acknowledged for molecular modeling. K.-L.C. and Y.-C.C. thank the financial support from the National Science and Technology Council in Taiwan (NSTC 111-2628-E-011-008-MY3) for supporting device fabrication and testing. A portion of morphology characterization was done at the Molecular Foundry, which is supported by the Office of Science, Office of Basic Energy Sciences, of the U.S. Department of Energy under Contract No. DE-AC02-05CH11231.

16163028, 0, Downloaded from https://onlinelibrary.wiley.com/doi/10.1002/adfm.202306576 by Univ of California Lawrence Berkeley National Lab, Wiley Online Library on [28/11/2023]. See the Terms and Conditions (https://onlinelibrary.wiley on Wiley Online Library for rules of use; OA articles are governed by the applicable Creative Common

Conflict of Interest

The authors declare no conflict of interest.

Data Availability Statement

The data that support the findings of this study are available from the corresponding author upon reasonable request.

Keywords

chain alignment mechanism, deformable rigid glassy conjugated polymers, mechanical properties of conjugated polymer thin films

Received: June 10, 2023 Revised: July 14, 2023 Published online:

- [1] D. Son, J. Kang, O. Vardoulis, Y. Kim, N. Matsuhisa, J. Y. Oh, J. W. To, J. Mun, T. Katsumata, Y. Liu, A. F. McGuire, M. Krason, F. Molina-Lopez, J. Ham, U. Kraft, Y. Lee, Y. Yun, J. B. H. Tok, Z. Bao, *Nat. Nanotechnol.* 2018, 13, 1057.
- [2] D. Son, J. Lee, S. Qiao, R. Ghaffari, J. Kim, J. E. Lee, C. Song, S. J. Kim, D. J. Lee, S. W. Jun, S. Yang, M. Park, J. Shin, K. Do, M. Lee, K. Kang, C. S. Hwang, N. Lu, T. Hyeon, D. H. Kim, Nat. Nanotechnol. 2014, 9, 397.
- [3] G. Schwartz, B. C. K. Tee, J. Mei, A. L. Appleton, D. H. Kim, H. Wang, Z. Bao, *Nat. Commun.* 2013, 4, 1859.
- [4] S. Wang, J. Y. Oh, J. Xu, H. Tran, Z. Bao, Acc. Chem. Res. 2018, 51, 1033.
- [5] Y. Jiang, Z. Zhang, Y. X. Wang, D. Li, C. T. Coen, E. Hwaun, G. Chen, H. C. Wu, D. Zhong, S. Niu, W. Wang, A. Saberi, J. C. Lai, Y. Wu, Y. Wang, A. A. Trotsyuk, K. Y. Loh, C. C. Shih, W. Xu, K. Liang, K. Zhang, Y. Bai, G. Gurusankar, W. Hu, W. Jia, Z. Cheng, R. H. Dauskardt, G. C. Gurtner, J. B. H. Tok, K. Deisseroth, et al., Science 2022, 375, 1411.
- [6] C. Zhu, Z. Bao, SID Symp. Dig. Tech. Pap. 2021, 52, 1052.
- [7] C. Larson, B. Peele, S. Li, S. Robinson, M. Totaro, L. Beccai, B. Mazzolai, R. Shepherd, *Science* 2016, 351, 1071.
- [8] M. S. White, M. Kaltenbrunner, E. D. Głowacki, K. Gutnichenko, G. Kettlgruber, I. Graz, S. Aazou, C. Ulbricht, D. A. M. Egbe, M. C. Miron, Z. Major, M. C. Scharber, T. Sekitani, T. Someya, S. Bauer, N. S. U. Sariciftci, Nat. Photonics 2013, 7, 811.
- [9] M. Kaltenbrunner, M. S. White, E. D. Głowacki, T. Sekitani, T. Someya, N. S. Sariciftci, S. Bauer, *Nat. Commun.* 2012, 3, 770.
- [10] T. Q. Trung, N. E. Lee, Adv. Mater. 2017, 29, 1603167.
- [11] A. X. Chen, A. T. Kleinschmidt, K. Choudhary, D. J. Lipomi, Chem. Mater. 2020, 32, 7582.
- [12] L. Janasz, M. Borkowski, P. W. M. Blom, T. Marszalek, W. Pisula, Adv. Funct. Mater. 2022, 32, 2105456.
- [13] Y. Zheng, S. Zhang, J. B.-H. Tok, Z. Bao, J. Am. Chem. Soc. 2022, 144, 4699.
- [14] P. Wang, J. Yang, Y. Zhang, W. Hu, H. Dong, ACS Mater. Lett. 2022, 4, 1112.
- [15] F. Wu, Y. Liu, J. Zhang, S. Duan, D. Ji, H. Yang, Small Methods 2021, 5, 2100676.
- [16] M. Ashizawa, Y. Zheng, H. Tran, Z. Bao, Prog. Polym. Sci. 2020, 100, 101181.
- [17] D. C. Kim, H. J. Shim, W. Lee, J. H. Koo, D. H. Kim, Adv. Mater. 2020, 32, 1902743.
- [18] G. J. N. Wang, A. Gasperini, Z. Bao, Adv. Electron. Mater. 2018, 4, 1700429.

- [19] B. Roth, S. Savagatrup, N. V. De Los Santos, O. Hagemann, J. E. Carlé, M. Helgesen, F. Livi, E. Bundgaard, R. R. Søndergaard, F. C. Krebs, D. J. Lipomi, *Chem. Mater.* 2016, 28, 2363.
- [20] J. Mun, G. J. N. Wang, J. Y. Oh, T. Katsumata, F. L. Lee, J. Kang, H. C. Wu, F. Lissel, S. Rondeau-Gagné, J. B. H. Tok, Z. Bao, Adv. Funct. Mater. 2018, 28, 1804222.
- [21] S. Savagatrup, X. Zhao, E. Chan, J. Mei, D. J. Lipomi, Macromol. Rapid Commun. 2016, 37, 1623.
- [22] J. Y. Oh, S. Rondeau-Gagné, Y. C. Chiu, A. Chortos, F. Lissel, G. J. N. Wang, B. C. Schroeder, T. Kurosawa, J. Lopez, T. Katsumata, J. Xu, C. Zhu, X. Gu, W. G. Bae, Y. Kim, L. Jin, J. W. Chung, J. B. H. Tok, Z. Bao, Nature 2016, 539, 411.
- [23] S. E. Root, S. Savagatrup, A. D. Printz, D. Rodriquez, D. J. Lipomi, Chem. Rev. 2017, 117, 6467.
- [24] Y. Zheng, M. Ashizawa, S. Zhang, J. Kang, S. Nikzad, Z. Yu, Y. Ochiai, H. C. Wu, H. Tran, J. Mun, Y. Q. Zheng, J. B. H. Tok, X. Gu, Z. Bao, *Chem. Mater.* 2020, 32, 5700.
- [25] Y. Zhao, X. Zhao, Y. Zang, C. A. Di, Y. Diao, J. Mei, Macromolecules 2015, 48, 2048.
- [26] X. Zhao, Y. Zhao, Q. Ge, K. Butrouna, Y. Diao, K. R. Graham, J. Mei, Macromolecules 2016, 49, 2601.
- [27] Y. Zhao, X. Zhao, M. Roders, A. Gumyusenge, A. L. Ayzner, J. Mei, Adv. Mater. 2017, 29, 1605056.
- [28] C. Müller, S. Goffri, D. W. Breiby, J. W. Andreasen, H. D. Chanzy, R. A. J. Janssen, M. M. Nielsen, C. P. Radano, H. Sirringhaus, P. Smith, N. T. Stingelin-Stutzmann, Adv. Funct. Mater. 2007, 17, 2674.
- [29] K. Ditte, J. Perez, S. Chae, M. Hambsch, M. Al-Hussein, H. Komber, P. Formanek, S. C. B. Mannsfeld, A. Fery, A. Kiriy, F. Lissel, Adv. Mater. 2021, 33, 2005416.
- [30] S. Zhang, M. U. Ocheje, L. Huang, L. Galuska, Z. Cao, S. Luo, Y. Cheng, D. Ehlenberg, R. B. Goodman, D. Zhou, Y. Liu, Y. Chiu, J. D. Azoulay, S. Rondeau-Gagné, X. Gu, Adv. Electron. Mater. 2019, 5, 1800899.
- [31] K. Sato, Y. Hemmi, A. Kato, H. Matsui, K. Fuchise, T. Higashihara, Polymer 2022, 252, 124934.
- [32] R. Peng, B. Pang, D. Hu, M. Chen, G. Zhang, X. Wang, H. Lu, K. Cho, L. Qiu, J. Mater. Chem. C 2015, 3, 3599.
- [33] L. C. Hsu, S. Kobayashi, T. Isono, Y. C. Chiang, B. J. Ree, T. Satoh, W. C. Chen, *Macromolecules* 2020, 53, 7496.
- [34] D. Liu, J. Mun, G. Chen, N. J. Schuster, W. Wang, Y. Zheng, S. Nikzad, J. C. Lai, Y. Wu, D. Zhong, Y. Lin, Y. Lei, Y. Chen, S. Gam, J. W. Chung, Y. Yun, J. B. H. Tok, Z. Bao, J. Am. Chem. Soc. 2021, 143, 11679.
- [35] F. Sugiyama, A. T. Kleinschmidt, L. V. Kayser, D. Rodriquez, M. Finn, M. A. Alkhadra, J. M. H. Wan, J. Ramírez, A. S. C. Chiang, S. E. Root, S. Savagatrup, D. J. Lipomi, *Polym. Chem.* 2018, 9, 4354.
- [36] H.-C. Yen, Y.-C. Lin, W.-C. Chen, Macromolecules 2021, 54, 1665.
- [37] S. Zhang, A. Alesadi, G. T. Mason, K. L. Chen, G. Freychet, L. Galuska, Y. H. Cheng, P. B. J. St Onge, M. U. Ocheje, G. Ma, Z. Qian, S. Dhakal, Z. Ahmad, C. Wang, Y. C. Chiu, S. Rondeau-Gagné, W. Xia, X. Gu, Adv. Funct. Mater. 2021, 31, 2100161.
- [38] Y. C. Chiang, H. C. Wu, H. F. Wen, C. C. Hung, C. W. Hong, C. C. Kuo, T. Higashihara, W. C. Chen, *Macromolecules* **2019**, *52*, 4396.
- [39] D. Liu, Z. Ding, Y. Wu, S. F. Liu, Y. Han, K. Zhao, *Macromolecules* **2022**, 55, 297
- [40] S. Zhang, Y. Cheng, L. Galuska, A. Roy, M. Lorenz, B. Chen, S. Luo, Y. Li, C. Hung, Z. Qian, P. B. J. St. Onge, G. T. Mason, L. Cowen, D. Zhou, S. I. Nazarenko, R. F. Storey, B. C. Schroeder, S. Rondeau-Gagné, Y. Chiu, X. Gu, Adv. Funct. Mater. 2020, 30, 2000663.
- [41] D. Choi, H. Kim, N. Persson, P. H. Chu, M. Chang, J. H. Kang, S. Graham, E. Reichmanis, Chem. Mater. 2016, 28, 1196.
- [42] S. Nikzad, H. C. Wu, J. Kim, C. M. Mahoney, J. R. Matthews, W. Niu, Y. Li, H. Wang, W. C. Chen, M. F. Toney, M. He, Z. Bao, *Chem. Mater.* 2020, 32, 897.



www.advancedsciencenews.com

FUNCTIONAL

16163028, 0, Downloaded from https://onlinelibrary.wiley.com/doi/10.1002/adfm.202306576 by Univ

of California Lawrence Berkeley National Lab, Wiley Online Library on [28/11/2023]. See the Terms

on Wiley Online Library for rules of

use; OA articles

www.afm-journal.de

- [43] Y. C. Chiang, C. C. Shih, S. H. Tung, W. C. Chen, Polymer 2018, 155, 146.
- [44] P. Kulatunga, N. Yousefi, S. Rondeau-Gagné, Chemosensors 2022, 10, 201.
- [45] M. Shin, J. Y. Oh, K. E. Byun, Y. J. Lee, B. Kim, H. K. Baik, J. J. Park, U. Jeong, Adv. Mater. 2015, 27, 1255.
- [46] J. Xu, S. Wang, G. J. N. Wang, C. Zhu, S. Luo, L. Jin, X. Gu, S. Chen, V. R. Feig, J. W. F. To, S. Rondeau-Gagné, J. Park, B. C. Schroeder, C. Lu, J. Y. Oh, Y. Wang, Y. H. Kim, H. Yan, R. Sinclair, D. Zhou, G. Xue, B. Murmann, C. Linder, W. Cai, J. B. H. Tok, J. W. Chung, Z. Bao, Science 2017. 355, 59.
- [47] Y. Zheng, G. J. N. Wang, J. Kang, M. Nikolka, H. C. Wu, H. Tran, S. Zhang, H. Yan, H. Chen, P. Y. Yuen, J. Mun, R. H. Dauskardt, I. McCulloch, J. B. H. Tok, X. Gu, Z. Bao, Adv. Funct. Mater. 2019, 29, 1905340.
- [48] A. Pawlak, A. Galeski, Macromolecules 2005, 38, 9688.
- [49] S. Zhang, M. Koizumi, Z. Cao, K. S. Mao, Z. Qian, L. A. Galuska, L. Jin, X. Gu, ACS Polym. Au 2021, 1, 16.
- [50] S. Zhang, L. A. Galuska, X. Gu, J. Polym. Sci. 2022, 60, 1108.
- [51] L. A. Galuska, W. W. McNutt, Z. Qian, S. Zhang, D. W. Weller, S. Dhakal, E. R. King, S. E. Morgan, J. D. Azoulay, J. Mei, X. Gu, Macro-molecules 2020, 53, 6032.
- [52] S. Zhang, M. U. Ocheje, S. Luo, D. Ehlenberg, B. Appleby, D. Weller, D. Zhou, S. Rondeau-Gagné, X. Gu, Macromol. Rapid Commun. 2018, 39, 1800092.
- [53] N. Balar, J. J. Rech, R. Henry, L. Ye, H. Ade, W. You, B. T. O'Connor, Chem. Mater. 2019, 31, 5124.
- [54] J. Choi, W. Kim, D. Kim, S. Kim, J. Chae, S. Q. Choi, F. S. Kim, T. S. Kim, B. J. Kim, Chem. Mater. 2019, 31, 3163.
- [55] P. Arasaratnam, K. S. Sivakumaran, M. J. Tait, ISRN Civ. Eng. 2011, 2011. 656401.
- [56] S.-A. Chen, J.-M. Ni, Macromolecules 1992, 25, 6081.
- [57] A. M. Fenton, R. Xie, M. P. Aplan, Y. Lee, M. G. Gill, R. Fair, F. Kempe, M. Sommer, C. R. Snyder, E. D. Gomez, R. H. Colby, ACS Cent. Sci. 2022, 8, 268.
- [58] M. A. Alkhadra, S. E. Root, K. M. Hilby, D. Rodriquez, F. Sugiyama, D. J. Lipomi, *Chem. Mater.* **2017**, *29*, 10139.
- [59] M. F. Butler, A. M. Donald, A. J. Ryan, Polymer 1998, 39, 39.

- [60] B. O'Connor, R. J. Kline, B. R. Conrad, L. J. Richter, D. Gundlach, M. F. Toney, D. M. DeLongchamp, Adv. Funct. Mater. 2011, 21, 3697.
- [61] B. T. O'Connor, O. G. Reid, X. Zhang, R. J. Kline, L. J. Richter, D. J. Gundlach, D. M. Delongchamp, M. F. Toney, N. Kopidakis, G. Rumbles, Adv. Funct. Mater. 2014, 24, 3422.
- [62] W. Y. Huang, C. C. Lee, S. G. Wang, Y. K. Han, M. Y. Chang, J. Electrochem. Soc. 2010, 157, B1336.
- [63] A. Shafiee, M. M. Salleh, M. Yahaya, Sains Malays. 2011, 40, 173.
- [64] T. Lei, Y. Cao, Y. Fan, C. Liu, S. Yuan, J. Pei, J. Am. Chem. Soc. 2011, 133, 6099.
- [65] A. Salleo, R. J. Kline, D. M. DeLongchamp, M. L. Chabinyc, Adv. Mater. 2010, 22, 3812.
- [66] R. J. Pandolfi, D. B. Allan, E. Arenholz, L. Barroso-Luque, S. I. Campbell, T. A. Caswell, A. Blair, F. De Carlo, S. Fackler, A. P. Fournier, G. Freychet, M. Fukuto, D. Gürsoy, Z. Jiang, H. Krishnan, D. Kumar, R. J. Kline, R. Li, C. Liman, S. Marchesini, A. Mehta, A. T. N'Diaye, D. Y. Parkinson, H. Parks, L. A. Pellouchoud, T. Perciano, F. Ren, S. Sahoo, J. Strzalka, D. Sunday, et al., J. Synchrotron Radiat. 2018, 25, 1261.
- [67] G. Freychet, Y. Huang, W. L. Tan, P. A. Gilhooly-Finn, C. B. Nielsen, H. Sirringhaus, C. R. McNeill, ACS Mater. Lett. 2022, 4, 764.
- [68] G. Freychet, E. Gann, M. Zhernenkov, C. R. McNeill, J. Phys. Chem. Lett. 2021, 12, 3762.
- [69] G. Freychet, E. Gann, L. Thomsen, X. Jiao, C. R. McNeill, J. Am. Chem. Soc. 2021, 143, 1409.
- [70] M. C. Gurau, D. M. Delongchamp, B. M. Vogel, E. K. Lin, D. A. Fischer, S. Sambasivan, L. J. Richter, *Langmuir* 2007, 23, 834.
- [71] Z. Li, Y. Liao, Y. Zhang, Y. Zhang, W. Xia, Extreme Mech. Lett. 2022, 50, 101519
- [72] Z. Ding, D. Liu, K. Zhao, Y. Han, Macromolecules 2021, 54, 3907.
- [73] R. Noriega, J. Rivnay, K. Vandewal, F. P. V. Koch, N. Stingelin, P. Smith, M. F. Toney, A. Salleo, *Nat. Mater.* 2013, 12, 1038.
- [74] Z. Zheng, K. H. Yim, M. S. M. Saifullah, M. E. Welland, R. H. Friend, J. S. Kim, W. T. S. Huck, *Nano Lett.* **2007**, *7*, 987.